



# Synergistic effect of $\text{Li}_2\text{MgTi}_3\text{O}_8$ coating layer with dual ionic surface doping to improve electrochemical performance of $\text{LiNi}_{0.6}\text{Co}_{0.2}\text{Mn}_{0.2}\text{O}_2$ cathode materials

Leiwu Tian<sup>1,2</sup> · Haifeng Yuan<sup>1,2</sup> · Qinjun Shao<sup>1,2</sup> · Syed Danish Ali Zaidi<sup>1,2</sup> · Chong Wang<sup>1</sup> · Jian Chen<sup>1</sup>

Received: 8 May 2020 / Revised: 3 June 2020 / Accepted: 14 June 2020 / Published online: 20 June 2020  
© Springer-Verlag GmbH Germany, part of Springer Nature 2020

## Abstract

Surface modification plays a vital role in improving the rate performance and cycling stability of layered Ni-rich  $\text{LiNi}_{0.6}\text{Co}_{0.2}\text{Mn}_{0.2}\text{O}_2$  (NCM622) cathode materials for Li-ion batteries. In this study,  $\text{Li}_2\text{MgTi}_3\text{O}_8$  (LMTO)-coated NCM622 was successfully synthesized by wet coating combined with sintering process. The results of morphological analysis showed a uniform LMTO layer coated on the surface of NCM622 materials. The dual ions of  $\text{Ti}^{4+}$  and  $\text{Mg}^{2+}$  on surface structure of NCM622 were identified by X-ray diffraction and X-ray photoelectron spectroscopy. The surface coating layer prevented the direct contact between the active cathode material and the electrolyte which significantly reduced the side reactions, and the doping of  $\text{Ti}^{4+}$  and  $\text{Mg}^{2+}$  improved the structural stability of the NCM622 materials. The electrochemical performance indicates that NCM622 cathode with a coating layer of 0.5 wt% LMTO exhibited excellent cycle stability and maintained a capacity retention up to 76% after 200 cycles at 25 °C at 1 C-rate, which was higher than the value of 52% for the NCM622.

**Keywords** Lithium-ion battery ·  $\text{LiNi}_{0.6}\text{Co}_{0.2}\text{Mn}_{0.2}\text{O}_2$  ·  $\text{Li}_2\text{MgTi}_3\text{O}_8$  · Surface coating · Surface doping

## Introduction

In facing with the increasing energy demands and environmental pollution caused by fossil energy, the development of sustainable energy storage system has become more and more critical. Rechargeable Li-ion batteries have been widely applied in electric vehicles, portable electronic devices, and aerospace industries due to their high energy density and low self-discharge [1–3]. However, the conventional Li-ion battery prepared with  $\text{LiCoO}_2$  cathode material could not satisfy

the increasing demands of high specific energy, low cost, and high safety [4, 5]. The layered Ni-rich cathode materials ( $\text{LiNi}_x\text{Co}_y\text{Mn}_z\text{O}_2$ ,  $x \geq 0.6$ ,  $x + y + z = 1$ ) have drawn much attention among the various advanced cathode materials, i.e.,  $\text{LiCoO}_2$ ,  $\text{LiFePO}_4$ ,  $\text{LiMn}_2\text{O}_4$ , and  $\text{LiNi}_{1.5}\text{Mn}_{0.5}\text{O}_4$ , owing to its higher energy density, lower price, and thermal stability [6]. Unfortunately, the Ni-rich cathode materials have always been encountered with some critical challenges such as ion mixing, structural instability, and residual lithium that limit its practical applications. Concerning the ion mixing, the Ni-rich cathode materials exhibit R3m structure where lithium ion locates at 3b sites and the transition metal ion locates at 3a sites. Because the radius of  $\text{Ni}^{2+}$  is 0.069 nm, which is similar to 0.076 nm for  $\text{Li}^+$  [7],  $\text{Ni}^{2+}$  ions can easily migrate from 3a sites to 3b sites and cause the ion mixing during the charge/discharge cycling process. The presence of  $\text{Ni}^{2+}$  in the lithium layer will hinder the diffusion of lithium ions in the bulk phase, which accelerates cathode material structure deterioration and battery capacity fading eventually [6]. As for the structural stability, the crystal structure of the Ni-rich cathode material converts from the layered phase (R3m) to the spinel-like phase (Fd3m) and rock-salt phase (Fm3m) after a long charge/discharge cycles [6, 8]. It will lead to a symmetric

**Electronic supplementary material** The online version of this article (<https://doi.org/10.1007/s11581-020-03665-8>) contains supplementary material, which is available to authorized users.

✉ Chong Wang  
wangchong@dicp.ac.cn

✉ Jian Chen  
chenjian@dicp.ac.cn

<sup>1</sup> Advanced Rechargeable Battery Laboratory, Dalian National Laboratory for Clean Energy, Dalian Institute of Chemical Physics, Chinese Academy of Sciences, Zhongshan Road 457, Dalian 116023, Liaoning, China

<sup>2</sup> University of Chinese Academy of Sciences, Beijing 100049, China

expansion and contraction of the cathode materials, which is responsibility for the generation of microcracks [9]. Meanwhile, the new generated Fm3m phase at the surface of cathode materials reduces the ionic conductivity and obstructs lithium-ion diffusion between the cathode and electrolyte. Besides, the residual lithium, such as  $\text{Li}_2\text{CO}_3$  and  $\text{LiOH}$ , is usually found on the surface of Ni-rich cathode materials due to the surface reactions of cathode materials with the moisture and  $\text{CO}_2$  in the air. The residual lithium will react with electrolyte that triggers a series of side reactions, such as forming cathode-electrolyte interface layer, and releasing gas to cause the severe safety issues [10]. In addition, the electrolyte decomposition can be accelerated due to the highly reactive  $\text{Ni}^{4+}$  contained in the delithiated Ni-rich cathode materials, which causes a depletion in active material and electrolytes with capacity fading [11]. As mentioned above, ion mixing, structure instability, and residual lithium are the main reasons for the poor stability of the Ni-rich cathode materials.

Many methods have been employed to overcome the problems mentioned above and improve the electrochemical stability of Ni-rich cathode materials. Various ions such as  $\text{Mg}^{2+}$  [12],  $\text{Ti}^{4+}$  [13],  $\text{Sn}^{4+}$  [14],  $\text{Al}^{3+}$  [15], and  $\text{Zn}^{4+}$  [16] were employed as the doping elements to improve the electrochemical performances of Ni-rich cathode materials. It was revealed that the ion doping could change the valence states, increase the strength of the transition metal–oxide bond, suppress the cation mixing and structure degradation, improve the ionic and electronic conductivity of the Ni-rich cathode materials, and prevent the side reactions [16, 17]. The surface coating is an effective method to avoid the direct contact and the side reactions between the cathode material and the organic electrolyte, keeping a crystalline structure of cathode materials with the improved electrochemical performance [6]. Therefore, many materials were introduced to modify Ni-rich cathode materials, such as metal oxide [18–22], active electrode materials [23–27], and carbon materials [28–30]. Meanwhile, both doping and surface coating were also applied to figure out the problems of Ni-rich cathode materials such as Mg doping and  $\text{Al}_2\text{O}_3$  coating [31], Mg doping and  $\text{Li}_3\text{PO}_4$  coating [32], Ce doping and  $\text{Ce}_{0.8}\text{Dy}_{0.2}\text{O}_{1.9}$  coating [33], and Y doping and  $\text{LiYO}_2$  coating [34]. In addition, other methods are also used in enhancing the electrochemical performance of Ni-rich cathode materials, like core-shell structure [35], gradient structure [36], porous structure [37], and electrode additive [38].

Spinel  $\text{Li}_4\text{Ti}_5\text{O}_{12}$ , a zero-strain material, has been widely applied as the coating material to improve the performance of electrode material due to its electrochemical inertness and the excellent structural stability. Xu et al. reported that  $\text{Li}_4\text{Ti}_5\text{O}_{12}$  coating layer significantly improved the cycle stability of  $\text{LiNi}_{0.8}\text{Co}_{0.1}\text{Mn}_{0.1}\text{O}_2$  cathode at high cutoff voltage [39]. Zhao et al. used a solvothermal method to coat  $\text{Li}_4\text{Ti}_5\text{O}_{12}$  on the surface of  $\text{LiNi}_{0.5}\text{Mn}_{1.5}\text{O}_4$

material. This coated materials exhibited enhanced interface stability [40].  $\text{Li}_2\text{MgTi}_3\text{O}_8$  (LMTO) possesses the same structure and chemical stability as  $\text{Li}_4\text{Ti}_5\text{O}_{12}$ , but the chemical diffusion coefficient of Li-ion in  $\text{Li}_2\text{MgTi}_3\text{O}_8$  is larger than that in  $\text{Li}_4\text{Ti}_5\text{O}_{12}$  due to the doping of Mg [41]. To our knowledge,  $\text{Li}_2\text{MgTi}_3\text{O}_8$  has not been used as a coating material to improve the electrochemical performance of Ni-rich materials.

In this work, we introduced simultaneous  $\text{Li}_2\text{MgTi}_3\text{O}_8$  surface coating and Ti/Mg dual surface doping using a wet coating method to improve the electrochemical performance of  $\text{LiNi}_{0.6}\text{Co}_{0.2}\text{Mn}_{0.2}\text{O}_2$ . The investigation in terms of morphology characteristic and electrochemical tests was carried out. The results indicate that  $\text{Li}_2\text{MgTi}_3\text{O}_8$  coating layer could inhibit the side reaction of the battery, and Ti/Mg dual surface doping could strengthen the structure stability and promote the diffusion of  $\text{Li}^+$ .

## Experimental

### Materials

Commercial  $\text{LiNi}_{0.6}\text{Co}_{0.2}\text{Mn}_{0.2}\text{O}_2$  (NCM622) was used as the cathode material as received.  $\text{C}_4\text{H}_6\text{O}_4\text{Mg}\cdot 4\text{H}_2\text{O}$  (99%) and  $\text{C}_2\text{H}_3\text{O}_2\text{Li}\cdot 2\text{H}_2\text{O}$  (99%) were provided by Aladdin.  $\text{Ti}(\text{OCH}(\text{CH}_3)_2)_4$  (99%) was supplied by Acros Organics. The electrolyte contains  $1.0 \text{ mol L}^{-1}$   $\text{LiPF}_6$  in a mixture solution of dimethyl carbonate (DMC), ethyl methyl carbonate (EMC), and ethylene carbonate (EC) (1:1:1 in volume) which was purchased from Zhangjiagang Guotai Huarong Co., China.

### Synthesis of the $\text{Li}_2\text{MgTi}_3\text{O}_8$ -coated $\text{LiNi}_{0.6}\text{Co}_{0.2}\text{Mn}_{0.2}\text{O}_2$

To prepare the samples with  $\text{Li}_2\text{MgTi}_3\text{O}_8$  (LMTO) coating layer, a stoichiometric ratio of starting materials, including  $\text{C}_4\text{H}_6\text{O}_4\text{Mg}\cdot 4\text{H}_2\text{O}$ ,  $\text{C}_2\text{H}_3\text{O}_2\text{Li}\cdot 2\text{H}_2\text{O}$ , and  $\text{Ti}(\text{OCH}(\text{CH}_3)_2)_4$ , was dissolved in 30 mL anhydrous ethanol and stirred for 30 min at 25 °C. The NCM622 powder was added into the solution and stirred overnight. Then, the above solution was stirred at 80 °C in the water bath until the ethanol was fully evaporated. Finally, the resulting sample was dried at 80 °C for 12 h and subsequently sintered at 750 °C for 8 h in air. The amounts of LMTO were set to 0.5, 1.0, and 3.0 wt% relative to the NCM622 powders, which is denoted as L0.5-NCM, L1.0-NCM, and L3.0-NCM, respectively. The resultant materials were collected after cooling down to room temperature. The schematic illustration of the synthesis process is showed in Fig. 1.

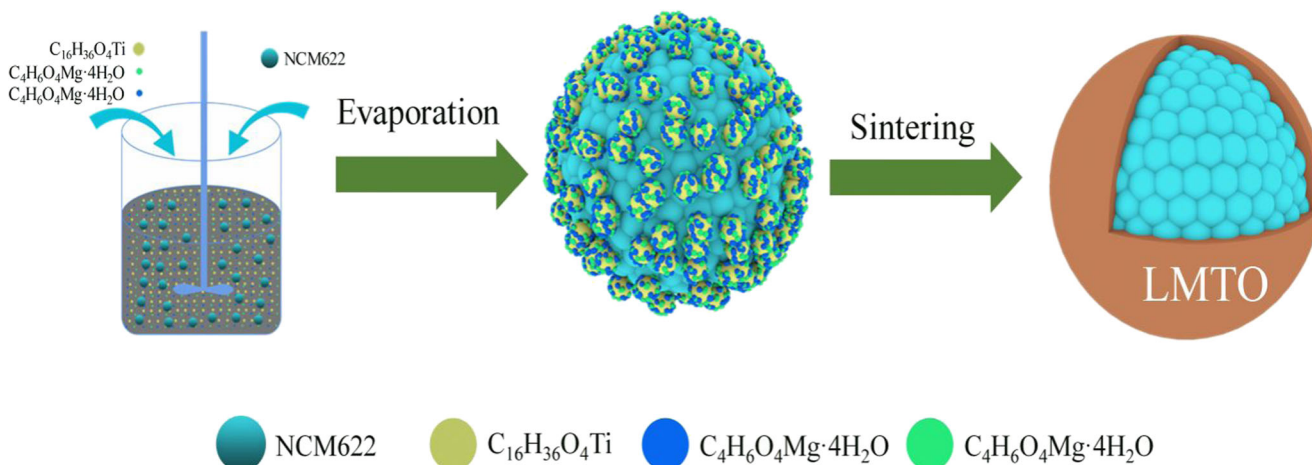


**Fig. 1** The schematic illustration shows the process of the LMTO coating layer on the NCM622 particle surface

### Material characterizations

The crystalline structures of the pristine and LMTO-coated NCM622 powders were identified by X-ray diffraction (PANalytical X'Pert PRO) with a scanning speed of  $1.17^\circ \text{ min}^{-1}$  with Cu K $\alpha$  radiation operated at 40 kV and 40 mA ( $\lambda = 1.5418 \text{ \AA}$ ). The Rietveld method was used to refine the lattice parameters (GSAS Rietveld program). Field emission scanning electron microscopy (FESEM, JSM-7800F) with energy dispersive spectroscope (EDS) mapping was conducted to study the surface particle morphology and element distributions. Transmission electron microscopy (TEM, JEM-2100) was used to characterize the micro-morphologies of the samples. The surface chemical valence states and element contents of the materials were identified by X-ray photoelectron spectroscopy (XPS, ESCALAB 250xi).

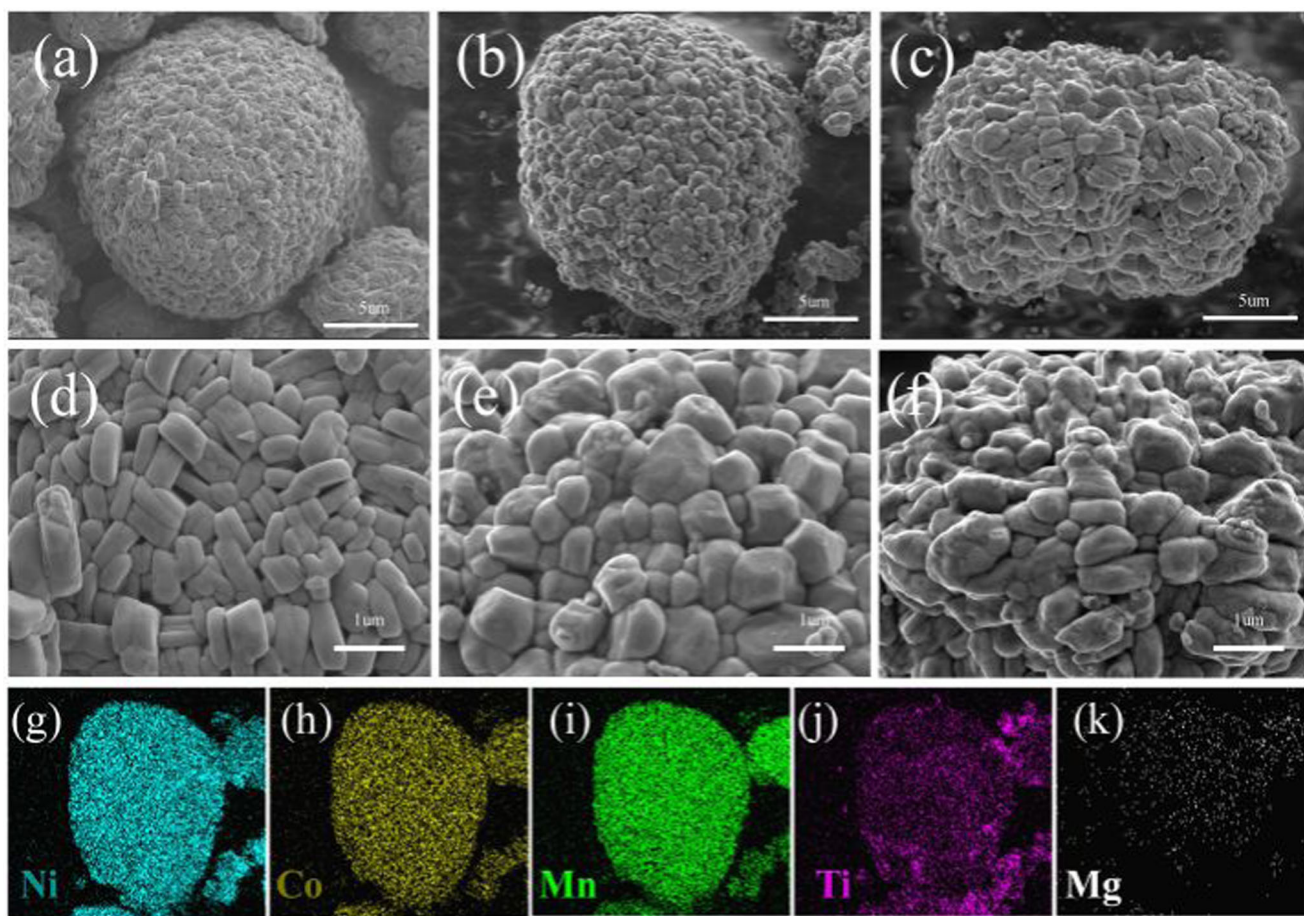
### Electrochemical tests

The cathode electrode composites were prepared by mixing the as-synthesized cathode materials, acetylene black (AB), and polyvinylidene fluoride (PVDF) binder with the weight ratio of 8:1:1. Then, the mixture was grinded to prepare the homogeneous slurry in N-methyl pyrrolidone (NMP) and casted onto aluminum foil using a doctor blade. The obtained electrodes were dried at  $75^\circ \text{C}$  for 8 h in a vacuum oven. Electrochemical measurements were performed by 2016 type coin cells, which were assembled in argon-fill glove. The lithium foil was used as the anode, 1 M LiPF<sub>6</sub> in a mixed solvent of DMC, EMC, and EC (1:1:1, v/v) was used as electrolyte, and the separator was Celgard 2500. The galvanostatic charge/discharge measurements were performed at room temperature in a potential range of 2.6–4.3 V using a battery test instrument (LAND CT-2001A, China) at different rates ( $1C = 277 \text{ mAh g}^{-1}$  based on the mass of active materials). Cyclic voltammetry (CV) was measured on the PARSTAT MC electrochemical workstation in the potential range of 2.6 to 4.3 V

at a scan rate of  $0.1 \text{ mV s}^{-1}$ . Electrochemical impedance spectroscopy (EIS) was recorded on the PARSTAT 1000 measurement system with amplitude of 5 mV in the frequency range of 100 kHz to 0.01 Hz.

### Results and discussion

The morphologies of NCM622, L0.5-NCM, L1.0-NCM, and L3.0-NCM powders at different magnifications were observed and recorded using SEM as shown in Fig. 2 and Fig. S1. All the samples present spherical morphology with the sizes of around  $10 \mu\text{m}$  in Fig. 2a, b and c. The spherical materials are consisted of plenty of primary particles in the size of 200–300 nm, indicating that the morphology of LMTO-coated cathode materials is almost unchanged. However, the coated samples (Fig. 2e and f) show rough surface, and the boundary between the primary crystals becomes unclear in comparison with the uncoated NCM622 (Fig. 2d), which is owing to the existence of the coating layers. The EDS mapping was used to investigate the uniformity of the coating layer and the element distribution of Ni, Co, Mn, Ti, and Mg for L0.5-NCM as shown in Fig. 2g–k. It displays that Ti and Mg are uniformly distributed, illustrating that the LMTO layer is successfully and uniformly coated on the surface of cathode materials. The TEM images of the L0.5-NCM as shown in Fig. 3a and b exhibit that the coating layer is in thickness of about 4 nm on the surface of L-0.5NCM particles. The magnified image in Fig. 3b clearly shows a lattice spacing of 0.245 nm which represented the (101) planes of NCM622. Moreover, new planes with lattice space of 0.223 and 0.241 nm are observed on the surface of L0.5-NCM, which are related to the (123) and (222) planes of Li<sub>2</sub>MgTi<sub>3</sub>O<sub>8</sub> (JCPDS No. 89-1308). Thus, it can be concluded that the NCM622 particles are uniformly coated with a thin layer of LMTO.

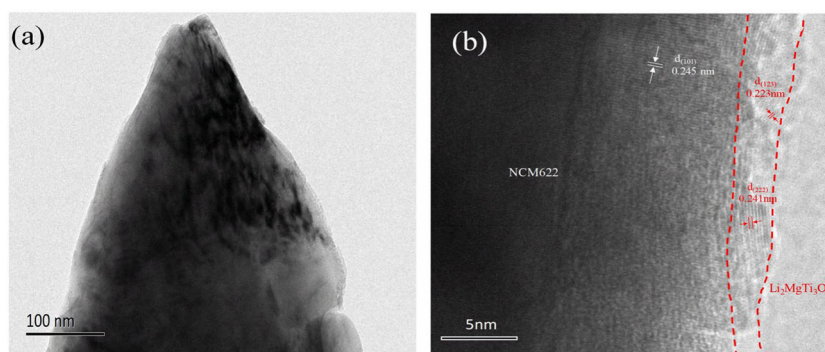


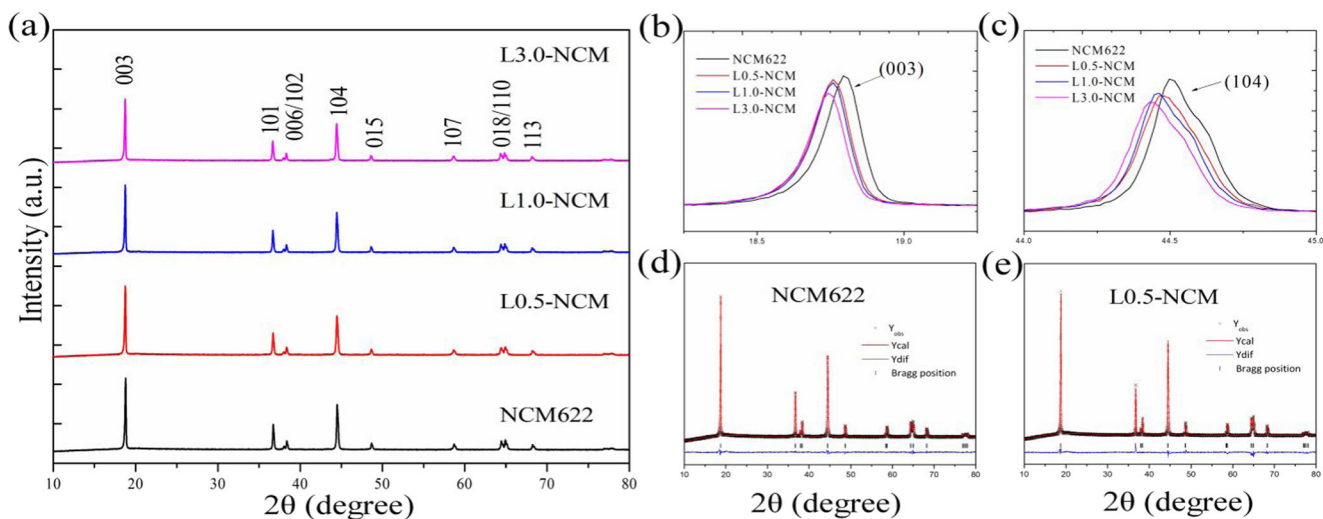
**Fig. 2** The SEM images of NCM622 (a, d), 0.5%-NCM (b, e), and 1%-NCM (c, f); the elemental mapping of L0.5-NCM for Ni (g), Co (h), Mn (i), Ti (j), and Mg (k)

Figure 4 shows X-ray powder diffraction (XRD) patterns of the pristine and LMTO-coated NCM622. As shown in Fig. 4a, all samples present similar diffraction patterns, which is a typical hexagonal  $\alpha$ - $\text{NaFeO}_2$  structure with the space group R3m without any impurities. The peak splitting of the (006)/(102) and (018)/(110) pairs can be clearly observed in Fig. S2 (a and b), indicating that all the samples possess a well-ordered layered structure. The values for  $I_{003}/I_{104}$  and  $c/a$  are important factors to reflect the degree of structural orderliness in the layered

materials. As displayed in Table 1, the  $I_{003}/I_{104}$  and  $c/a$  values are larger than 1.2 and 4.9, respectively, suggesting that all samples exhibit a lower degree of  $\text{Li}^+/\text{Ni}^{2+}$  mixing and well-ordered layer structure [42, 43]. The magnified (003) and (104) peaks (Fig. 4b and c) of the LMTO-coated samples shift to a lower angle compared with the NCM622, indicating that the structure has been changed. This phenomenon is possibly caused by the migration of the  $\text{Mg}^{2+}$  and  $\text{Ti}^{4+}$  from the coating layer to the surface structure of NCM622 materials via solid-state diffusion

**Fig. 3** TEM images of L0.5-NCM (a, b)





**Fig. 4** a XRD patterns of the related samples; b, c the magnification peaks of (003) and (104); d, e the XRD Rietveld refinement of NCM622 and L0.5-NCM

during the sintering process. Rietveld refinements (GSAS) were used to identify the crystal constant difference of the samples presented in Fig. 4d and e and Fig. S2 (c and d), and the calculation results are shown in Table 1. The lattice parameters of *c* and unit volume for the LMTO-coated materials are increased compared with the pristine NCM622. This is due to the charge compensation for  $Ti^{4+}$  doping in sintering process, in which  $Ni^{3+}$  ions can be reduced to  $Ni^{2+}$  [44]. The ionic radius of  $Ni^{2+}$  ion is 0.069 nm, which is larger than  $Ni^{3+}$  ion of 0.060 nm. The increased amount of the larger  $Ni^{2+}$  ions can enlarge the lattice parameters that ultimately accelerates the  $Li^+$  insertion/extraction into/from the lattice of NCM622 [32, 39, 45]. The ionic radius of  $Ti^{4+}$  ion is 0.0605 nm, which is similar as 0.060 nm for  $Ni^{3+}$  ion. The ionic radius for  $Mg^{2+}$  and  $Li^+$  is 0.072 nm and 0.076 nm, respectively. Thus, it is very likely that  $Ti^{4+}$  ions can occupy in the transition metal layer and  $Mg^{2+}$  ions occupy in the Li layer [39, 46, 47]. The occupation of  $Mg^{2+}$  ions in the Li layer could inhibit the migration of  $Ni^{2+}$  to Li layer, thus reducing the ion mixing [47, 48]. This result is supported by the smaller  $I_{003}/I_{104}$  value of NCM622 (1.597) in comparison with L0.5-NCM (1.734), L1.0-NCM (1.697), and L3.0-NCM (1.607) in Table 1. In addition, the doping of  $Mg^{2+}$  ions could stabilize the structural

stability of the layered NCM622 through the pillar effect, which enhances the cycle performance of the cathode materials [49].

XPS was used to further investigate the chemical states of Ni, Co, Mn, Ti, and Mg ions on the surface of the prepared samples. Figure 5a shows Ni  $2p_{3/2}$  spectrum and the fitted results (XPSPEAK software) of the pristine and the LMTO-coated samples. The Ni  $2p_{3/2}$  peak for pristine NCM622 locates at 855.40 eV, and its two sets of peaks locate at 854.50 eV and 855.80 eV, corresponding to the binding energies of  $Ni^{2+}$  and  $Ni^{3+}$ . As can be seen, the Ni  $2p_{3/2}$  peak for LMTO-coated samples gradually shifts to lower binding energy at 855.24, 855.09, and 854.06 eV for L0.5-NCM, L1.0-NCM, and L3.0-NCM with the increased amount of coating materials. Moreover, the peak area is associated with the quantity of various  $Ni^{2+}/Ni^{3+}$  oxidation states [11]. The fitted results show that the contents of  $Ni^{2+}$  increase from 23.40 to 30.49%, 38.9%, and 37.05% for NCM622, L0.5-NCM, L1.0-NCM, and L3.0-NCM. These results are consistent with the XRD tests that  $Ni^{3+}$  ions are reduced to  $Ni^{2+}$  due to the doping of  $Ti^{4+}$  [44]. The increase of  $Ni^{2+}$  concentration could improve the structural stability of cathode materials [50]. Figure 5b shows that Ti 2p has two peaks at 458.20 eV and 464.0 eV for LMTO-coated NCM622 material, corresponding to Ti  $2p_{3/2}$  and Ti  $2p_{1/2}$ , respectively. Both peaks indicate that the

**Table 1** Structural parameters obtained from Rietveld refinement of XRD pattern of the related samples

	<i>a</i> (Å)	<i>c</i> (Å)	<i>c/a</i>	Unit volume (Å <sup>3</sup> )	<i>R</i> <sub>wp</sub> (%)	<i>I</i> <sub>(003)/ (104)</sub>
NCM622	2.87251	14.21622	4.94904	101.588	1.72	1.597
L0.5-NCM	2.87248	14.22419	4.95264	101.642	1.39	1.734
L1.0-NCM	2.87325	14.21967	4.94898	101.664	1.79	1.697
L3.0-NCM	2.87449	14.22882	4.95002	101.817	1.70	1.670

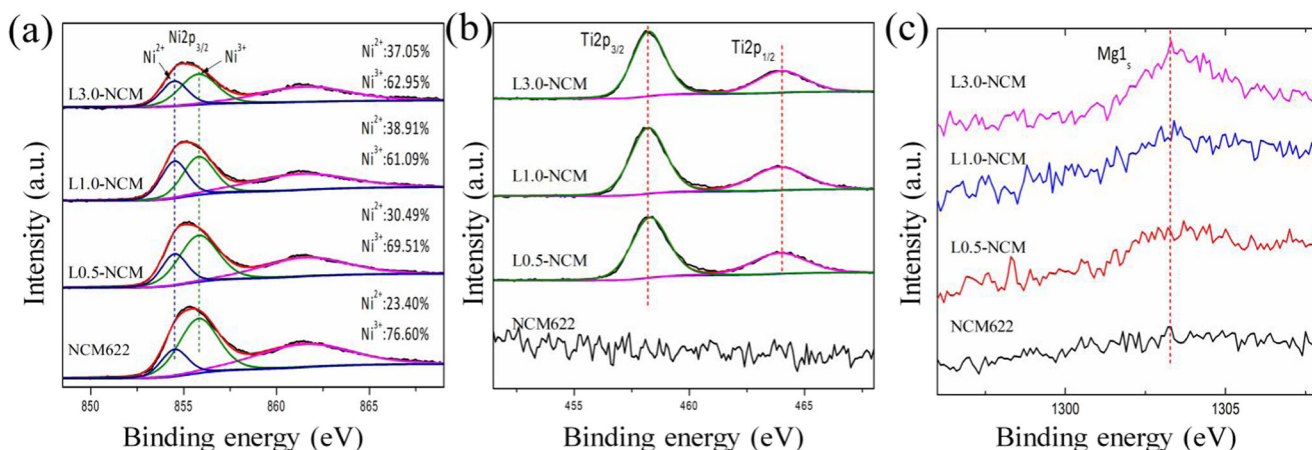


**Fig. 5** XPS spectrum of Ni (a), Ti (b), and Mg (c)

Ti ions are mainly in an oxidation state with valence state of +4. Figure 5c displays the Mg 1s peak. The binding energy of Mg 1s is around 1303.3 eV, and the increased intensity of Mg 1s means the increased contents of Mg ions. The main peaks of 2p<sub>3/2</sub> and 2p<sub>1/2</sub> for Co and Mn are observed at 780.20 and 795.10, 642.30, and 654.03 eV as shown in Fig. S3 (a and b), indicating that the Co ions and Mn ions are mainly in an oxidation state with valence state of +3 and +4.

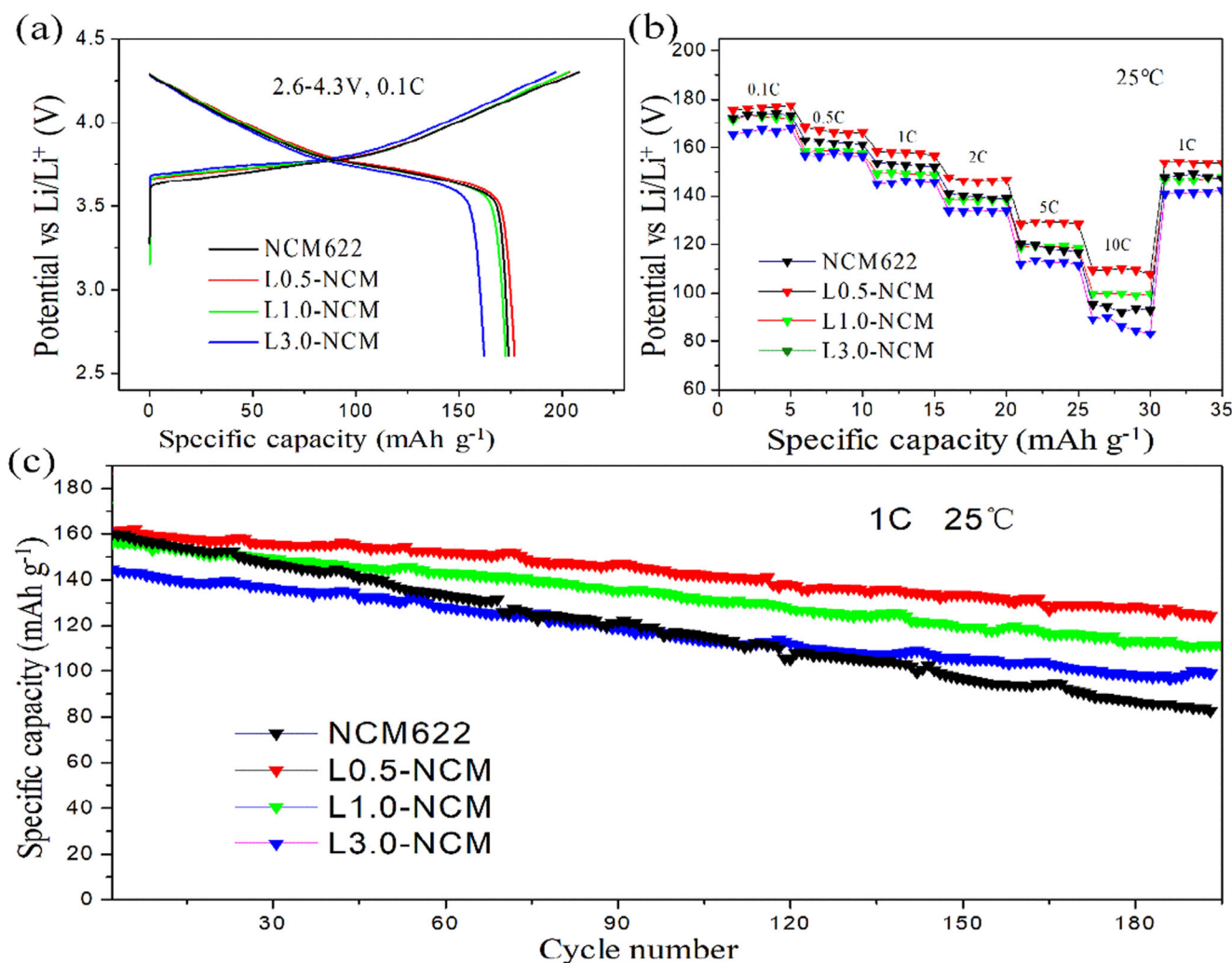
To study the influence of LMTO coating on the electrochemical properties of NCM622 materials, the related samples were tested by galvanostatic charge/discharge measurements in the voltage range of 2.6–4.3 V (vs. Li/Li<sup>+</sup>). Figure 6a displays the first charge/discharge curves of both the pristine and the coated NCM622 materials at 0.1C (1C = 277 mAh g<sup>-1</sup>). The profiles obtained with the coated samples are consistent with the uncoated NCM622. There is no other phase that can be observed, indicating that the LMTO is electrochemically inactive in the working voltage range. The first discharge capacities of NCM622, L0.5-NCM, L1.0-NCM, and L3.0-NCM are recorded as 174.0, 175.1, 172.6, and 162.1 mAh g<sup>-1</sup>, respectively. It can be seen that the L0.5-NCM shows higher discharge capacity than the NCM622, which is mainly due to the LMTO coating layer that significantly decreases the polarization and suppresses the side reactions between the cathode surface and the electrolyte [51, 52]. However, the L1.0-NCM and L3.0-NCM show a slight lower discharge capacity than the NCM622, possibly due to the increase mass amount of electrochemically inactive LMTO on cathode materials.

Figure 6b compares the rate capabilities of the pristine and the coated NCM622 materials at various current rates from 0.1 C to 10 C and then back to 1 C. The L0.5-NCM shows better rate properties than the NCM622 and other LMTO-coated samples. The specific capacities for L0.5-NCM are obtained as 175.4, 168.4, 158.5, 147.7, 128.3, and 109.5 mAh g<sup>-1</sup> at 0.1, 0.5, 1.0, 2.0, 5.0, and 10.0 C, respectively. The NCM622 exhibits 172.3, 163.1, 153.7, 141.2, 120.0, and 95.2 mAh g<sup>-1</sup> at the same conditions as that for L0.5-NCM. The capacity

retention of L0.5-NCM at 10 C remains about 62% of the capacity at 0.1 C, which is larger than 55% obtained with the NCM622. Figure S4 shows the charge/discharge curves of the pristine NCM622 and L0.5-NCM as well as the corresponding dQ/dV plots at different rates. It can be observed that the overpotential increases with the rise of the discharge current and the dQ/dV minima gradually shift to lower voltage. The voltage difference of the NCM622 is 0.221 V between 0.1 C and 10 C, which is larger than 0.143 V obtained with the L0.5-NCM. The significant enhanced rate performance originates from the expansion of lattice parameters caused by doping of Ti and Mg, which have been proved by XRD tests [53].

The cycle performance test was utilized to further study the effect of coating layers on NCM cathode materials. All the samples were cycled galvanostatically at 1 C for 200 cycles after pre-activation at 0.1 C for the first cycle. As can be seen from Fig. 6c, the L0.5-NCM exhibits the initial capacity of 163.8 mAh g<sup>-1</sup> at 1 C which is larger than 161.7, 156.1, and 144.6 mAh g<sup>-1</sup> for NCM622, L1.0-NCM, and L3.0-NCM, respectively. After 200 cycles, L0.5-NCM also displays the best cycling performance with a capacity retention of 76.8%, while the NCM622, L1.0-NCM, and L3.0-NCM retained of their initial discharge capacities about 52.0%, 70.4%, and 68.5%, respectively. These results indicate that LMTO coating could effectively improve the electrochemical performance of NCM622 materials. Conclusively, LMTO coating layer can reduce the contact and resistance between the electrolyte and the electrode and improve the reversibility of the Li-ion insertion/deintercalation reaction of the coated cathode.

To further investigate the enhanced electrochemical performance of LMTO-coated NCM, the charge/discharge profiles for the NCM622 and L0.5-NCM at 1st, 50th, 100th, 150th, and 200th cycles have been analyzed and depicted in Fig. 7a and c, and the corresponding dQ/dV curves are shown in Fig. 7b and d. The gaps between the charge/discharge plateaus and the difference in oxidation peak are caused by the structure change from layered phase to rock-salt phase during charge/



**Fig. 6** Initial charge/discharge voltage profiles at 0.1C (a), rate performance of related samples (b); cycle performance of related samples at 1.0C (c)

discharge process The L0.5-NCM shows a narrow gap and a small oxidation peak difference (0.017 V) between 1st and 200th in comparison with the pristine NCM622 (0.134 V), indicating that LMTO coating layer could reduce the polarization and voltage fading in the long-term cycling test [52]. Thus, the specific capacity and cyclic stability of LMTO-coated samples could be improved.

CV plots of the NCM622 and L0.5-NCM between 2.6 and 4.3 V at a scan rate of 0.1 mV s<sup>-1</sup> are shown in Fig. 8a and b. The curves exhibit similar shapes with a couple of redox peaks appeared in the scanning voltage range which corresponded to the oxidation and reduction of Ni<sup>2+</sup>/Ni<sup>3+</sup> and Ni<sup>4+</sup> [54]. The initial anodic and cathodic peaks of the NCM622 are 3.915 V and 3.703 V with a potential difference ( $\Delta E_p$ ) of 0.212 V in Fig. 8a. However, the peaks of the L0.5-NCM are 3.838 V and 3.713 V with a small  $\Delta E_p$  of 0.125 V in Fig. 8b, which demonstrated the lower polarization effect during the electrochemical reaction process for the L0.5-NCM. The reduced polarization of L0.5-NCM can be attributed to the improved reaction kinetics and minimized charge transfer resistance

during continuous charge/discharge process. It is resulted from the uniform coating layer of LMTO and Ti/Mg dual-ion doping, which facilitates the Li<sup>+</sup> transport and stabilizes the structure stability of cathode materials. It also demonstrates the better cycling and rate performance of the L0.5-NCM.

To further clarify the structural integrity of the samples, XRD patterns and electrode morphology after 100 cycles are analyzed in Fig. 9. As can be seen in Fig. 9a and b, it is distinctly observed that the secondary particles of the NCM622 break to small pieces after cycles, while the L0.5-NCM electrode shows intact morphology without any crack in Fig. 9c and d. Figure 9e shows the XRD patterns of the NCM622 and L0.5-NCM after 100 cycles. The  $I_{(003)}/I_{(104)}$  ratio of the NCM622 (1.26) is much lower than that of L0.5-NCM (1.63), which confirms that the LMTO modification could maintain the layer structure of the cathode materials. The SEM and XRD results after cycles are consistent with the analysis of electrochemical performance test that LMTO coating and Ti/Mg dual

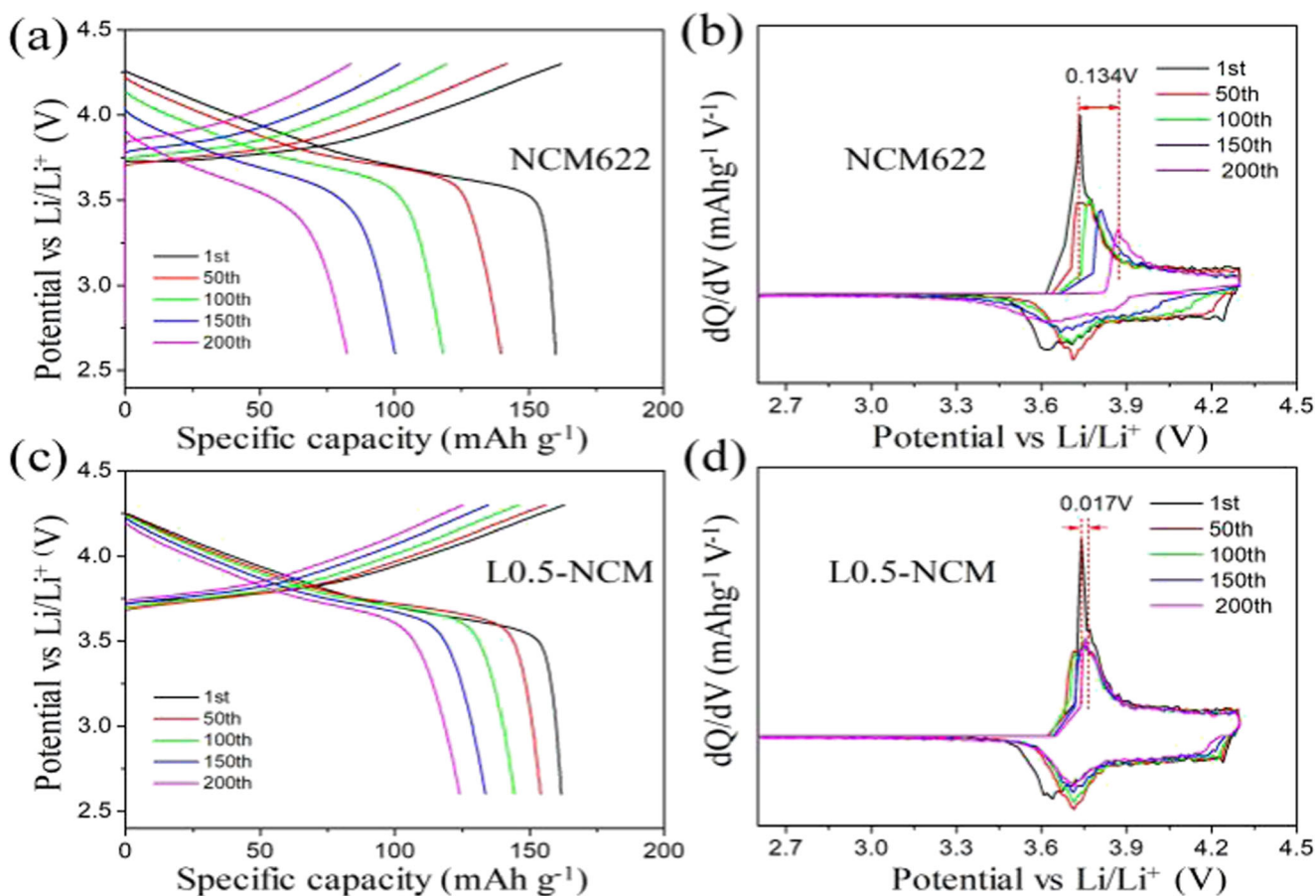


**Fig. 7** The specific capacity vs. voltage curves of NCM622 (a) and 0.5%-NCM (b). The dQ/dV curves of NCM622 (c) and 0.5%-NCM (d) cycled at 1C

doping can stabilize the surface structure and suppress the surface reconstruction of NCM622 cathode materials [39].

The EIS measurements are used to investigate the deep reasons of improved electrochemical performance of the LMTO-coated NCM622 material. The EIS tests were carried out for the NCM622 and L0.5-NCM in charge state (4.3 V) after the 1st and 100th cycles at

1.0 C. As can be seen in Fig. 10a and b, two depressed semicircles and a slope line are observed in the Nyquist plots for all electrodes. The semicircle located in high-frequency region was assigned to surface film resistance ( $R_{sf}$ ), which was related to the migration of Li-ion through the surface film. The semicircle located in middle-frequency region was assigned to charge transfer

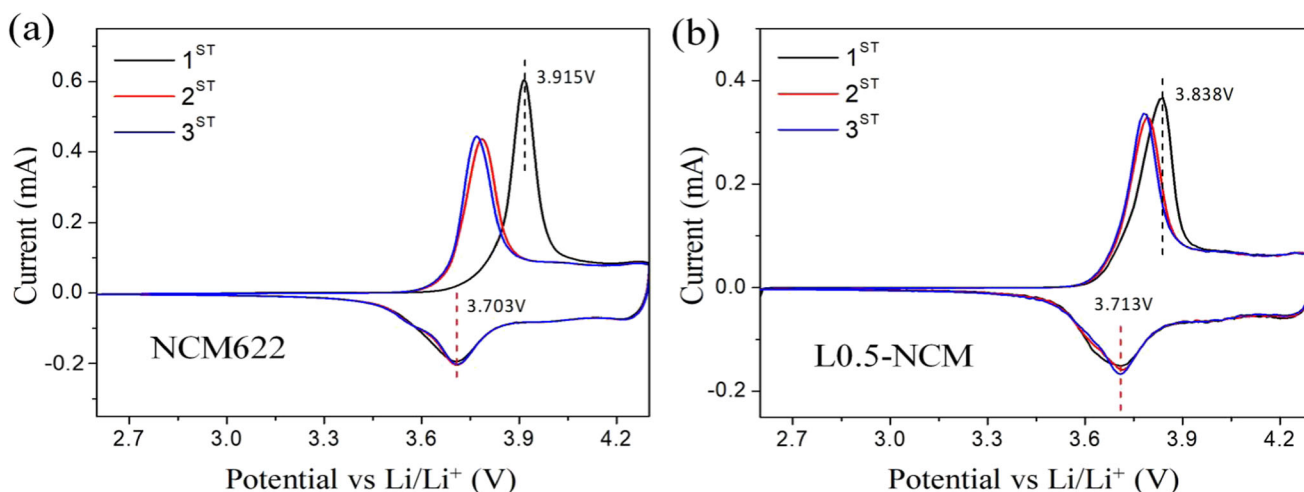


**Fig. 8** Cyclic voltammetry profiles of NCM622 (a) and L0.5-NCM (b) at the voltage range of 2.6–4.3 V and the scan rate of 0.1  $\text{mV s}^{-1}$



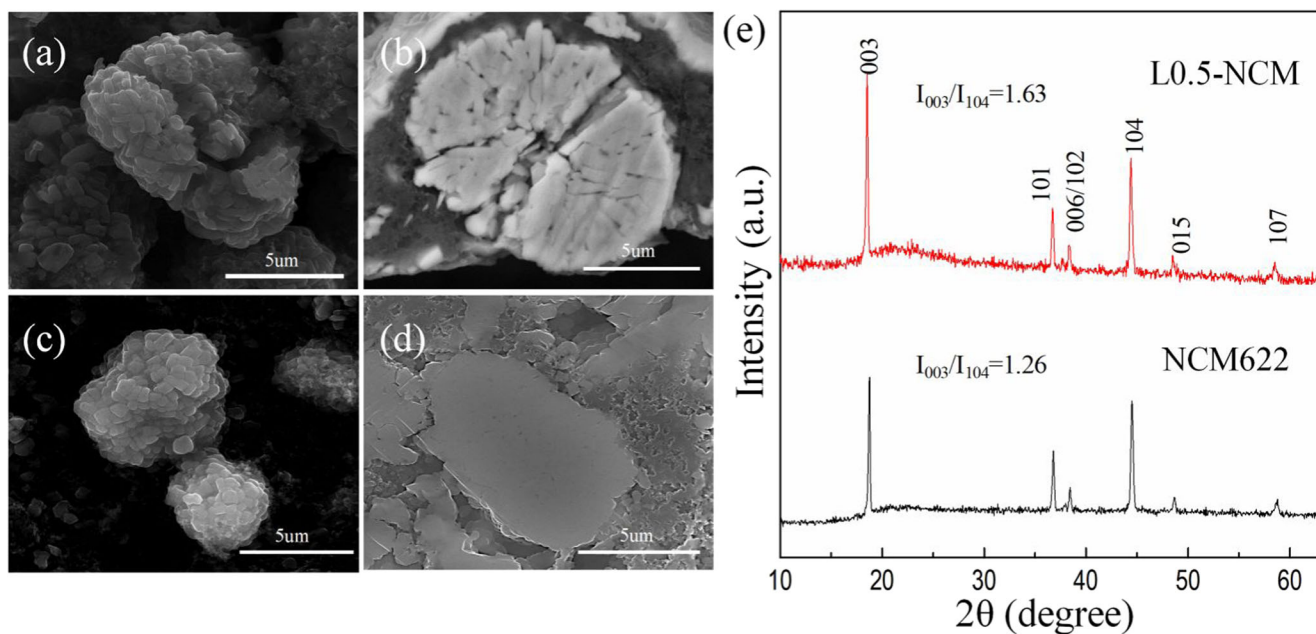


**Fig. 9** The electrode morphology of NCM622 (a) and L0.5-NCM (c) after 100 cycles. The cross-sectional morphology of NCM622 (b) and L0.5-NCM (d) after 100 cycles. The XRD patterns of NCM622 and L0.5-NCM after 100 cycles

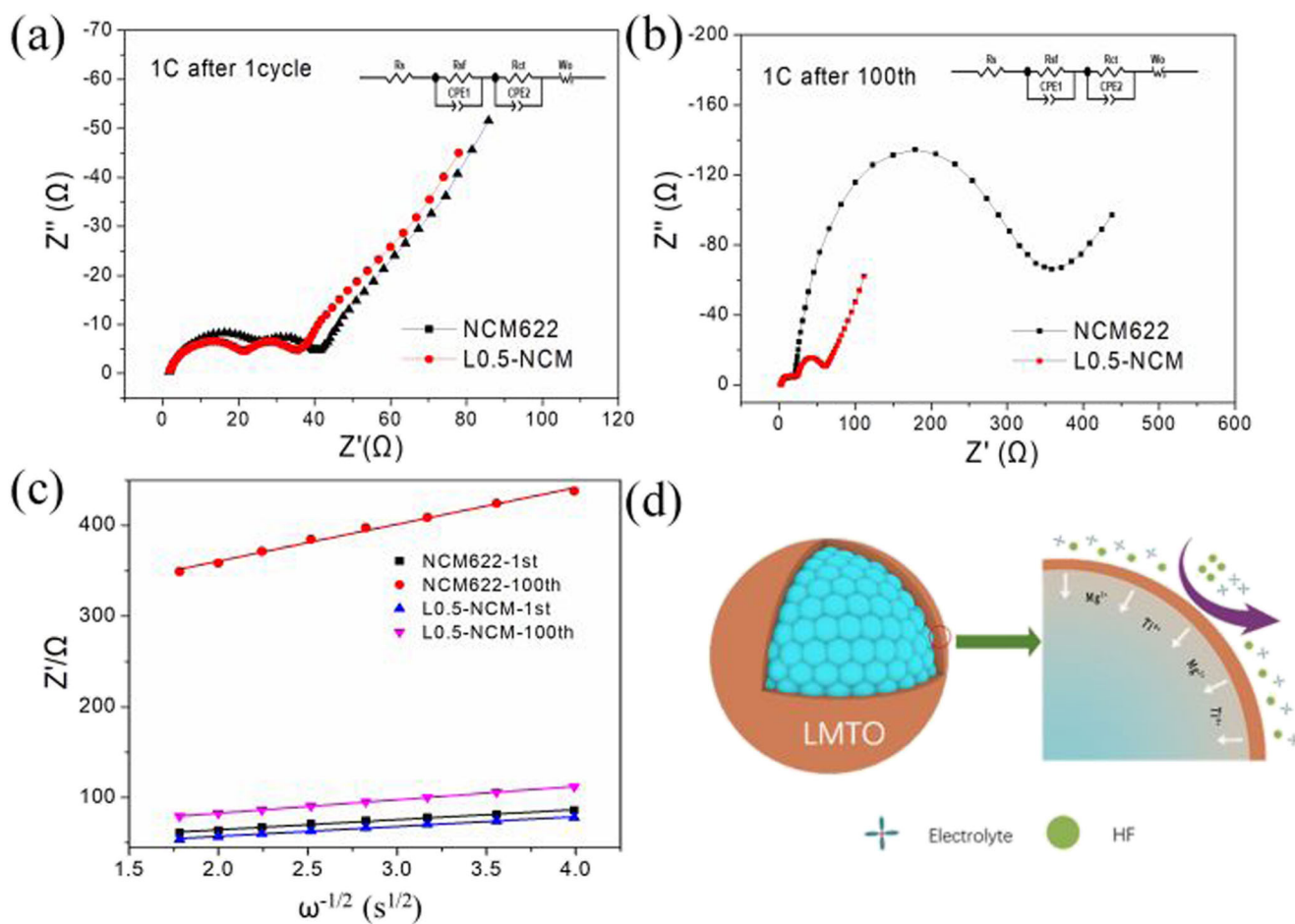


**Fig. 10** EIS spectra of NCM622 and L0.5-NCM at the 1st cycle (a) and 100th cycle (b) at charge state, and the inside graphics is the equivalent circuit model. Linear fitting graph of  $Z'-\omega^{-1/2}$  after 1st and 100th (c).

Schematic view of stronger structure stability and reduced side reaction of LMTO-coated NCM (d)

**Table 2** EIS fitting results and Li<sup>+</sup> ion diffusion coefficient of the NCM622 and L0.5-NCM

	At the 1st cycle			At the 100th cycle		
	$R_{sf}$	$R_{ct}$	$D_{Li}$ (cm <sup>2</sup> s <sup>-1</sup> )	$R_{sf}$	$R_{ct}$	$D_{Li}$ (cm <sup>2</sup> s <sup>-1</sup> )
NCM622	19.65	11.08	$4.63 \times 10^{-10}$	22.46	333.9	$3.51 \times 10^{-11}$
L0.5-NCM	22.11	8.523	$4.90 \times 10^{-10}$	26.54	28.1	$2.59 \times 10^{-10}$

impedance at the electrolyte/electrode interface ( $R_{ct}$ ). The slope line at the low-frequency region was related to Li<sup>+</sup> diffusion process in the electrode bulk material (Warburg impedance,  $W_o$ ) [55]. The Z-view software was used to simulate the experimental data and the results are listed in Table 2. The results show that there is no significant difference of  $R_{sf}$  and  $R_{ct}$  between the NCM622 and L0.5-NCM at the first cycle. However,  $R_{ct}$  values of the NCM622 and L0.5-NCM increase from 11.08  $\Omega$  and 8.523  $\Omega$  to 333.9  $\Omega$  and 28.1  $\Omega$  after 100 cycles, respectively. The increase of  $R_{ct}$  value of L0.5-NCM is significantly depressed, which is attributed to the surface ion doping and thin film coating. It improves the structure stability and decreases the reaction kinetics resistance. These results are defined well in agreement with the improvement of electrochemical performance. The following equation was used to calculate the lithium-ion diffusion coefficients ( $D_{Li}$ ) of pristine and coated materials [11, 56–58]:

$$D_{Li} = 0.5(RT/An^2F^2C\sigma)^2 \quad (1)$$

The value of  $R$ ,  $T$ , and  $F$  represents the gas constant (8.314 J K<sup>-1</sup> mol), absolute temperature (298.15 K), and Faraday constant (96,485.3383), respectively;  $A$  represents the surface area of the electrode (0.785 cm<sup>2</sup>);  $n$  is the react number of electrons ( $n = 1$ );  $C$  is the concentration of Li<sup>+</sup> in cathode material (0.001 mol cm<sup>-3</sup> in this work) [11, 56];  $\sigma$  represents the Warburg factor which is the slope of  $Z'-\omega^{-1/2}$  (Fig. 10c) and can be calculated by the following equation:

$$Z' = R_s + R_{ct} + \sigma\omega^{-1/2} \quad (2)$$

where  $Z'$  and  $\omega$  are real parts for impedance and angular frequency, respectively. The calculated values of Li<sup>+</sup> ion diffusion coefficient ( $D_{Li}$ ) are shown in Table 2. It shows that  $D_{Li}$  of the L0.5-NCM is  $4.90 \times 10^{-10}$  cm<sup>2</sup> s<sup>-1</sup> and  $2.59 \times 10^{-10}$  cm<sup>2</sup> s<sup>-1</sup> in the first cycle and 100 cycles, which are higher than the NCM622 of  $4.63 \times 10^{-10}$  cm<sup>2</sup> s<sup>-1</sup> and  $3.51 \times 10^{-11}$  cm<sup>2</sup> s<sup>-1</sup> in the same condition. The results indicate that the NCM622 with LMTO coating layer and Ti/Mg ion dual doping could promote the Li<sup>+</sup> diffusion, resulting in improved rate capability.

## Conclusions

In summary, a series of Li<sub>2</sub>MgTi<sub>3</sub>O<sub>8</sub>-coated LiNi<sub>0.6</sub>Co<sub>0.2</sub>Mn<sub>0.2</sub>O<sub>2</sub> cathode materials were fabricated by wet coating process. All the coated samples showed a pure hexagonal  $\alpha$ -NaFeO<sub>2</sub> phase with no significant impurity peak. The TEM, XPS, and XRD analysis showed that the NCM622 particles were successfully coated with thin LMTO layer and doped with Ti<sup>4+</sup> and Mg<sup>2+</sup>. The 0.5 wt% LMTO-coated NCM622 exhibited 76.8% of the capacity retention after 200 cycles, whereas pristine NCM622 showed a lower capacity retention ratio of 52%. This great improvement was mainly attributed to the LMTO coating layer and Ti/Mg dual doping, which not only helped in physically insulation between the cathode and the electrolyte but also improved the ionic transport kinetics and structure stability of NCM622 cathode.

**Authors' contributions** Conceptualization: Jian Chen, Chong Wang; methodology: Chong Wang; formal analysis and investigation: Leiwu Tian, Haifeng Yuan, Qinjun Shao; writing—original draft preparation: Leiwu Tian; writing—review and editing: Leiwu Tian, Syed Danish Ali Zaidi, Chong Wang; funding acquisition: Jian Chen; resources: Chong Wang; supervision: Chong Wang, Jian Chen.

**Funding information** This study was funded by the National Key R&D Program of China (2016YFB0100100) and Defense Industrial Technology Development Program (JCKY2018130C107).

**Data availability** The data that support the findings of this study are available from the corresponding author on request.

## Compliance with ethical standards

**Conflict of interest** The authors declare that they have no conflict of interest.

**Code availability** Not applicable

## References

1. Tarascon JM, Armand M (2001) Issues and challenges facing rechargeable lithium batteries. *Nature* 414(6861):359–367. <https://doi.org/10.1038/35104644>
2. Liu C, Li F, Ma LP, Cheng HM (2010) Advanced materials for energy storage. *Adv Mater* 22(8):E28–E62. <https://doi.org/10.1002/adma.200903328>
3. Goodenough JB, Park KS (2013) The Li-ion rechargeable battery: a perspective. *JACS* 135(4):1167–1176. <https://doi.org/10.1021/ja3091438>
4. Fu C, Li G, Luo D, Li Q, Fan J, Li L (2014) Nickel-rich layered microspheres cathodes: lithium/nickel disordering and electrochemical performance. *ACS Appl Energy Mater* 6(18):15822–15831. <https://doi.org/10.1021/am5030726>
5. Wang Q, Shen CH, Shen SY, Xu YF, Shi CG, Huang L, Li JT, Sun SG (2017) Origin of structural evolution in capacity degradation for overcharged NMC622 via operando coupled investigation. *ACS Appl Energy Mater* 9(29):24731–24742. <https://doi.org/10.1021/acsaami.7b06326>

6. Liu W, Oh P, Liu X, Lee M-J, Cho W, Chae S, Kim Y, Cho J (2015) Nickel-rich layered lithium transition-metal oxide for high-energy lithium-ion batteries. *Angew Chem Int Ed* 54(15):4440–4457. <https://doi.org/10.1002/anie.201409262>
7. Kim J, Lee H, Cha H, Yoon M, Park M, Cho J (2018) Prospect and reality of Ni-rich cathode for commercialization. *Adv Energy Mater* 8(6):1702028. <https://doi.org/10.1002/aenm.201702028>
8. Kim H, Kim MG, Jeong HY, Nam H, Cho J (2015) A new coating method for alleviating surface degradation of LiNi<sub>0.6</sub>Co<sub>0.2</sub>Mn<sub>0.2</sub>O<sub>2</sub> cathode material: nanoscale surface treatment of primary particles. *Nano Lett* 15(3):2111–2119. <https://doi.org/10.1021/acs.nanolett.5b00045>
9. Ran Q, Zhao H, Shu X, Hu Y, Hao S, Shen Q, Liu W, Liu J, Zhang M, Li H, Liu X (2019) Enhancing the electrochemical performance of Ni-rich layered oxide cathodes by combination of the gradient doping and dual-conductive layers coating. *ACS Appl Energy Mater* 2(5):3120–3130. <https://doi.org/10.1021/acsaem.8b02112>
10. Cho DH, Jo CH, Cho W, Kim YJ, Yashiro H, Sun YK, Myung ST (2014) Effect of residual lithium compounds on layer Ni-rich Li[Ni<sub>0.7</sub>Mn<sub>0.3</sub>]O<sub>2</sub>. *J Electrochem Soc* 161(6):A920–A926. <https://doi.org/10.1149/2.042406jes>
11. Zhang J, Zhang J, Ou X, Wang C, Peng C, Zhang B (2019) Enhancing high-voltage performance of Ni-rich cathode by surface modification of self-assembled NASICON fast ionic conductor LiZr<sub>2</sub>(PO<sub>4</sub>)<sub>3</sub>. *ACS Appl Energy Mater* 11(17):15507–15516. <https://doi.org/10.1021/acsaem.9b00389>
12. Huang Z, Wang Z, Zheng X, Guo H, Li X, Jing Q, Yang Z (2015) Effect of Mg doping on the structural and electrochemical performance of LiNi<sub>0.6</sub>Co<sub>0.2</sub>Mn<sub>0.2</sub>O<sub>2</sub> cathode materials. *Electrochim Acta* 182:795–802. <https://doi.org/10.1016/j.electacta.2015.09.151>
13. Yang HP, Wu HH, Ge MY, Li LJ, Yf Y, Yao Q, Chen J, Xia LF, Zheng JM, Chen ZY, Duan JF, Kisslinger K, Zeng XC, Lee WK, Zhang QB, Lu J (2019) Simultaneously dual modification of Ni-rich layered oxide cathode for high-energy lithium-ion batteries. *Adv Funct Mater* 29(13):1808825. <https://doi.org/10.1002/adfm.201808825>
14. Eilers-Rethwisch M, Hildebrand S, Evertz M, Ibing L, Dagger T, Winter M, Schappacher FM (2018) Comparative study of Sn-doped Li[Ni<sub>0.6</sub>Mn<sub>0.2</sub>Co<sub>0.2</sub>-xSn<sub>x</sub>]O<sub>2</sub> cathode active materials (x=0–0.5) for lithium ion batteries regarding electrochemical performance and structural stability. *J Power Sources* 397:68–78. <https://doi.org/10.1016/j.jpowsour.2018.06.072>
15. Eilers-Rethwisch M, Winter M, Schappacher FM (2018) Synthesis, electrochemical investigation and structural analysis of doped Li[Ni<sub>0.6</sub>Mn<sub>0.2</sub>Co<sub>0.2</sub>-M]O<sub>2</sub> (x = 0, 0.05; M = Al, Fe, Sn) cathode materials. *J Power Sources* 387:101–107. <https://doi.org/10.1016/j.jpowsour.2018.02.080>
16. Gao S, Zhan XW, Cheng YT (2019) Structural, electrochemical and Li-ion transport properties of Zr-modified LiNi<sub>0.8</sub>Co<sub>0.1</sub>Mn<sub>0.1</sub>O<sub>2</sub> positive electrode materials for Li-ion batteries. *J Power Sources* 410–411:45–52. <https://doi.org/10.1016/j.jpowsour.2018.10.094>
17. Weigel T, Schipper F, Erickson EM, Susai FA, Markovsky B, Aurbach D (2019) Structural and electrochemical aspects of LiNi<sub>0.8</sub>Co<sub>0.1</sub>Mn<sub>0.1</sub>O<sub>2</sub> cathode materials doped by various cations. *ACS Energy Letters* 4(2):508–516. <https://doi.org/10.1021/acsaenergylett.8b02302>
18. Shi Y, Zhang M, Qian D, Meng YS (2016) Ultrathin Al<sub>2</sub>O<sub>3</sub> coatings for improved cycling performance and thermal stability of LiNi<sub>0.5</sub>Co<sub>0.2</sub>Mn<sub>0.3</sub>O<sub>2</sub> cathode material. *Electrochim Acta* 203:154–161. <https://doi.org/10.1016/j.electacta.2016.03.185>
19. Gao H, Zeng X, Hu Y, Tileli V, Li L, Ren Y, Meng X, Maglia F, Lamp P, Kim S-J, Amine K, Chen Z (2018) Modifying the surface of a high-voltage lithium-ion cathode. *ACS Appl Energy Mater* 1(5):2254–2260. <https://doi.org/10.1021/acsaem.8b00323>
20. Hu SK, Cheng GH, Cheng MY, Hwang BJ, Santhanam R (2009) Cycle life improvement of ZrO<sub>2</sub>-coated spherical LiNi<sub>1/3</sub>Co<sub>1/3</sub>Mn<sub>1/3</sub>O<sub>2</sub> cathode material for lithium ion batteries. *J Power Sources* 188(2):564–569. <https://doi.org/10.1016/j.jpowsour.2008.11.113>
21. Luo W, Zheng B (2017) Improved electrochemical performance of LiNi<sub>0.5</sub>Co<sub>0.2</sub>Mn<sub>0.3</sub>O<sub>2</sub> cathode material by double-layer coating with graphene oxide and V<sub>2</sub>O<sub>5</sub> for lithium-ion batteries. *Appl Surf Sci* 404:310–317. <https://doi.org/10.1016/j.apsusc.2017.01.200>
22. Liu K, Yang GL, Dong Y, Shi T, Chen L (2015) Enhanced cycling stability and rate performance of Li[Ni<sub>0.5</sub>Co<sub>0.2</sub>Mn<sub>0.3</sub>]O<sub>2</sub> by CeO<sub>2</sub> coating at high cut-off voltage. *J Power Sources* 281:370–377. <https://doi.org/10.1016/j.jpowsour.2014.12.131>
23. Choi JW, Lee JW (2016) Improved electrochemical properties of Li(Ni<sub>0.6</sub>Mn<sub>0.2</sub>Co<sub>0.2</sub>)O<sub>2</sub> by surface coating with Li<sub>1.3</sub>Al<sub>0.3</sub>Ti<sub>1.7</sub>(PO<sub>4</sub>)<sub>3</sub>. *J Power Sources* 307:63–68. <https://doi.org/10.1016/j.jpowsour.2015.12.055>
24. Chen J, Zhu L, Jia D, Jiang X, Wu Y, Hao Q, Xia X, Ouyang Y, Peng L, Tang W, Liu T (2019) LiNi<sub>0.8</sub>Co<sub>0.15</sub>Al<sub>0.05</sub>O<sub>2</sub> cathodes exhibiting improved capacity retention and thermal stability due to a lithium iron phosphate coating. *Electrochim Acta* 312:179–187. <https://doi.org/10.1016/j.electacta.2019.04.153>
25. Li J, Liu Y, Yao W, Rao X, Zhong S, Qian L (2020) Li<sub>2</sub>TiO<sub>3</sub> and Li<sub>2</sub>ZrO<sub>3</sub> co-modification LiNi<sub>0.8</sub>Co<sub>0.1</sub>Mn<sub>0.1</sub>O<sub>2</sub> cathode material with improved high-voltage cycling performance for lithium-ion batteries. *Solid State Ionics* 349:115292. <https://doi.org/10.1016/j.ssi.2020.115292>
26. Guan P, Zhou L, Yu Z, Sun Y, Liu Y, Wu F, Jiang Y, Chu D (2020) Recent progress of surface coating on cathode materials for high-performance lithium-ion batteries. *J Energy Chem* 43:220–235. <https://doi.org/10.1016/j.jechem.2019.08.022>
27. Li X, Jin L, Song D, Zhang H, Shi X, Wang Z, Zhang L, Zhu L (2020) LiNbO<sub>3</sub>-coated LiNi<sub>0.8</sub>Co<sub>0.1</sub>Mn<sub>0.1</sub>O<sub>2</sub> cathode with high discharge capacity and rate performance for all-solid-state lithium battery. *J Energy Chem* 40:39–45. <https://doi.org/10.1016/j.jechem.2019.02.006>
28. Fan Q, Yang S, Liu J, Liu H, Lin K, Liu R, Hong C, Liu L, Chen Y, An K, Liu P, Shi Z, Yang Y (2019) Mixed-conducting interlayer boosting the electrochemical performance of Ni-rich layered oxide cathode materials for lithium ion batteries. *J Power Sources* 421:91–99. <https://doi.org/10.1016/j.jpowsour.2019.03.014>
29. Liu Z, Wang Z, Lu T, Dai P, Gao P, Zhu Y (2018) Modification of LiNi<sub>0.8</sub>Co<sub>0.15</sub>Al<sub>0.05</sub>O<sub>2</sub> using nanoscale carbon coating. *J Alloys Compd* 763:701–710. <https://doi.org/10.1016/j.jallcom.2018.06.016>
30. Dong H, Liu G, Li S, Deng S, Cui Y, Liu H, Liu H, Sun X (2018) Design of 3D porous structure with residual carbon for high-performance Ni-rich cathode materials. *ACS Appl Mater Interfaces* 11(2):2500–2506. <https://doi.org/10.1021/acsaem.8b17800>
31. Sun S, Liu T, Niu Q, Sun X, Song D, Liu H, Zhou X, Ohsaka T, Wu J (2019) Improvement of superior cycle performance of LiNi<sub>0.8</sub>Co<sub>0.15</sub>Al<sub>0.05</sub>O<sub>2</sub> cathode for lithium-ion batteries by multiple compound modifications. *J Electroanal Chem* 838:178–185. <https://doi.org/10.1016/j.jelechem.2019.03.009>
32. Chen T, Wang F, Li X, Yan X, Wang H, Deng B, Xie Z, Qu M (2019) Dual functional MgHPO<sub>4</sub> surface modifier used to repair deteriorated Ni-rich LiNi<sub>0.8</sub>Co<sub>0.15</sub>Al<sub>0.05</sub>O<sub>2</sub> cathode material. *Appl Surf Sci* 465:863–870. <https://doi.org/10.1016/j.apsusc.2018.09.250>
33. Wang L, Liu G, Ding X, Zhan C, Wang X (2019) Simultaneous coating and doping of a nickel-rich cathode by an oxygen ion conductor for enhanced stability and power of lithium-ion batteries. *ACS Appl Mater Interfaces* 11(37):33901–33912. <https://doi.org/10.1021/acsaem.9b10310>

34. Zhang M, Zhao H, Tan M, Liu J, Hu Y, Liu S, Shu X, Li H, Ran Q, Cai J, Liu X (2019) Yttrium modified Ni-rich  $\text{LiNi}_0.8\text{Co}_0.1\text{Mn}_0.1\text{O}_2$  with enhanced electrochemical performance as high energy density cathode material at 4.5 V high voltage. *J Alloys Compd* 774:82–92. <https://doi.org/10.1016/j.jallcom.2018.09.281>
35. Song D, Hou P, Wang X, Shi X, Zhang L (2015) Understanding the origin of enhanced performances in core-shell and concentration-gradient layered oxide cathode materials. *ACS Appl Mater Interfaces* 7(23):12864–12872. <https://doi.org/10.1021/acsami.5b02373>
36. Su Y, Chen G, Chen L, Lu Y, Zhang Q, Lv Z, Li C, Li L, Liu N, Tan G, Bao L, Chen S, Wu F (2019) High-rate structure-gradient Ni-rich cathode material for lithium-ion batteries. *ACS Appl Mater Interfaces* 11(40):36697–36704. <https://doi.org/10.1021/acsami.9b12113>
37. Su Y, Zhang Q, Chen L, Bao L, Lu Y, Shi Q, Wang J, Chen S, Wu F (2020) Improved stability of layered and porous nickel-rich cathode materials by relieving the accumulation of inner stress. *ChemSusChem* 13(2):426–433. <https://doi.org/10.1002/cssc.201902385>
38. Xue R, Liu N, Bao L, Chen L, Su Y, Lu Y, Dong J, Chen S, Wu F (2020) UiO-66 type metal-organic framework as a multifunctional additive to enhance the interfacial stability of Ni-rich layered cathode material. *J Energy Chem* 50:378–386. <https://doi.org/10.1016/j.jechem.2020.03.049>
39. Xu YD, Xiang W, Wu ZG, Xu CL, Li YC, Guo XD, Lv GP, Peng X, Zhong BH (2018) Improving cycling performance and rate capability of Ni-rich  $\text{LiNi}_0.8\text{Co}_0.1\text{Mn}_0.1\text{O}_2$  cathode materials by  $\text{Li}_4\text{Ti}_5\text{O}_{12}$  coating. *Electrochim Acta* 268:358–365. <https://doi.org/10.1016/j.electacta.2018.02.049>
40. Zhao J, Liu Y, He Y, Lu K (2019)  $\text{Li}_4\text{Ti}_5\text{O}_{12}$  epitaxial coating on  $\text{LiNi}_0.5\text{Mn}_1.5\text{O}_4$  surface for improving the electrochemical performance through solvothermal-assisted processing. *J Alloys Compd* 779:978–984. <https://doi.org/10.1016/j.jallcom.2018.11.152>
41. Lu J, Peng Q, Wang W, Nan C, Li L, Li Y (2013) Nanoscale coating of  $\text{LiMO}_2$  (M = Ni, Co, Mn) nanobelts with Li+conductive  $\text{Li}_2\text{TiO}_3$ : toward better rate capabilities for Li-ion batteries. *JACS* 135(5):1649–1652. <https://doi.org/10.1021/ja308717z>
42. Feng Z, Peng Z, Huang X, Rajagopalan R, Tang Y, Wang H (2019) Enhanced electrochemical properties of  $\text{LiNi}_0.8\text{Co}_0.1\text{Mn}_0.1\text{O}_2$  at elevated temperature by simultaneous structure and interface regulating. *J Electrochem Soc* 166(8):A1439–A1448. <https://doi.org/10.1149/2.0331908jes>
43. Zhang LL, Wang JQ, Yang XL, Liang G, Li T, Yu PL, Ma D (2018) Enhanced electrochemical performance of fast ionic conductor  $\text{LiTi}_2(\text{PO}_4)_3$ -coated  $\text{LiNi}_1/3\text{Co}_1/3\text{Mn}_1/3\text{O}_2$  cathode material. *ACS Appl Mater Interfaces* 10(14):11663–11670. <https://doi.org/10.1021/acsami.7b19692>
44. Wu F, Liu N, Chen L, Su Y, Tan G, Bao L, Zhang Q, Lu Y, Wang J, Chen S, Tan J (2019) Improving the reversibility of the H2-H3 phase transitions for layered Ni-rich oxide cathode towards retarded structural transition and enhanced cycle stability. *Nano Energy* 59:50–57. <https://doi.org/10.1016/j.nanoen.2019.02.027>
45. Li Q, Zhou D, Zhang L, Ning D, Chen Z, Xu Z, Gao R, Liu X, Xie D, Schumacher G, Liu X (2019) Tuning anionic redox activity and reversibility for a high-capacity Li-rich Mn-based oxide cathode via an integrated strategy. *Adv Funct Mater* 29(10):1806706. <https://doi.org/10.1002/adfm.201806706>
46. Cho J (2000)  $\text{LiNi}_0.74\text{Co}_0.26-x\text{Mg}_x\text{O}_2$  cathode material for a Li-ion cell. *Chem Mater* 12(10):3089–3094. <https://doi.org/10.1021/cm000153l>
47. Huang Z, Wang Z, Zheng X, Guo H, Li X, Jing Q, Yang Z (2015) Structural and electrochemical properties of Mg-doped nickel based cathode materials  $\text{LiNi}_0.6\text{Co}_0.2\text{Mn}_0.2-x\text{Mg}_x\text{O}_2$  for lithium ion batteries. *RSC Adv* 5(108):88773–88779. <https://doi.org/10.1039/c5ra16633k>
48. He T, Chen L, Su Y, Lu Y, Bao L, Chen G, Zhang Q, Chen S, Wu F (2019) The effects of alkali metal ions with different ionic radii substituting in Li sites on the electrochemical properties of Ni-rich cathode materials. *J Power Sources* 441:227195. <https://doi.org/10.1016/j.jpowsour.2019.227195>
49. Li H, Zhou P, Liu F, Li H, Cheng F, Chen J (2019) Stabilizing nickel-rich layered oxide cathodes by magnesium doping for rechargeable lithium-ion batteries. *Chem Sci* 10(5):1374–1379. <https://doi.org/10.1039/C8SC03385D>
50. Chen T, Li X, Wang H, Yan X, Wang L, Deng B, Ge W, Qu M (2018) The effect of gradient boracic polyanion-doping on structure, morphology, and cycling performance of Ni-rich  $\text{LiNi}_0.8\text{Co}_0.15\text{Al}_0.05\text{O}_2$  cathode material. *J Power Sources* 374:1–11. <https://doi.org/10.1016/j.jpowsour.2017.11.020>
51. Yang XQ, Tang ZF, Wang HY, Zou BK, Chen CH (2016) Improving the electrochemical performance of  $\text{LiNi}_0.5\text{Co}_0.2\text{Mn}_0.3\text{O}_2$  by double-layer coating with  $\text{Li}_2\text{TiO}_3$  for lithium-ion batteries. *Ionics* 22(11):2235–2238. <https://doi.org/10.1007/s11581-016-1792-0>
52. Wang M, Zhang R, Gong Y, Su Y, Xiang D, Chen L, Chen Y, Luo M, Chu M (2017) Improved electrochemical performance of the  $\text{LiNi}_0.8\text{Co}_0.1\text{Mn}_0.1\text{O}_2$  material with lithium-ion conductor coating for lithium-ion batteries. *Solid State Ionics* 312:53–60. <https://doi.org/10.1016/j.ssi.2017.10.017>
53. Wu F, Wang M, Su Y, Chen S, Xu B (2009) Effect of  $\text{TiO}_2$ -coating on the electrochemical performances of  $\text{LiCo}_1/3\text{Ni}_1/3\text{Mn}_1/3\text{O}_2$ . *J Power Sources* 191(2):628–632. <https://doi.org/10.1016/j.jpowsour.2009.02.063>
54. Song G, Zhong H, Dai Y, Zhou X, Yang J (2018)  $\text{WO}_3$  membrane-encapsulated layered  $\text{LiNi}_0.6\text{Co}_0.2\text{Mn}_0.2\text{O}_2$  cathode material for advanced Li-ion batteries. *Ceram Int*. <https://doi.org/10.1016/j.ceramint.2018.12.169>
55. Tang W, Chen Z, Xiong F, Chen F, Huang C, Gao Q, Wang T, Yang Z, Zhang W (2019) An effective etching-induced coating strategy to shield  $\text{LiNi}_0.8\text{Co}_0.1\text{Mn}_0.1\text{O}_2$  electrode materials by  $\text{LiAlO}_2$ . *J Power Sources* 412:246–254. <https://doi.org/10.1016/j.jpowsour.2018.11.062>
56. Zhang J, Cao Y, Ou X, Zhang J, Wang C, Peng C, Zhang B, Tian Y (2019) Constituting the NASICON type solid electrolyte coated material forming anti-high voltage system to enhance the high cut-off voltage performance of  $\text{LiNi}_0.6\text{Co}_0.2\text{Mn}_0.2\text{O}_2$  via charge attracts electrostatic assembly. *J Power Sources* 436:226722. <https://doi.org/10.1016/j.jpowsour.2019.226722>
57. Kong JZ, Ren C, Tai GA, Zhang X, Li AD, Wu D, Li H, Zhou F (2014) Ultrathin  $\text{ZnO}$  coating for improved electrochemical performance of  $\text{LiNi}_0.5\text{Co}_0.2\text{Mn}_0.3\text{O}_2$  cathode material. *J Power Sources* 266:433–439. <https://doi.org/10.1016/j.jpowsour.2014.05.027>
58. Wu J, Tan X, Zhang J, Guo L, Jiang Y, Liu S, Zhao T, Liu Y, Ren J, Wang H, Kang X, Chu W (2019) Improvement of electrochemical performance of nickel rich  $\text{LiNi}_0.8\text{Co}_0.1\text{Mn}_0.1\text{O}_2$  cathode by lithium aluminates surface modifications. *Energy Technol* 7(2):209–215. <https://doi.org/10.1002/ente.201800506>

**Publisher's note** Springer Nature remains neutral with regard to jurisdictional claims in published maps and institutional affiliations.